Measurement of $R_{\rm uds}$ and R between 3.12 and 3.72 GeV at the KEDR detector

V.V. Anashin[a], V.M. Aulchenko[a,b], E.M. Baldin[a,b], A.K. Barladyan[a], A.Yu. Barnyakov[a,b], M.Yu. Barnyakov[a,b], S.E. Baru[a,b], I.Yu. Basok[a], A.M. Batrakov[a], A.E. Blinov[a,b], V.E. Blinov[a,b,c], A.V. Bobrov[a,b], V.S. Bobrovnikov[a,b], A.V. Bogomyagkov[a,b], A.E. Bondar[a,b], A.A. Borodenko[a], A.R. Buzykaev[a,b], S.I. Eidelman[a,b], D.N. Grigoriev[a,b,c], Yu.M. Glukhovchenko[a], S.E. Karnaev[a], G.V. Karpov[a], S.V. Karpov[a], P.V. Kasyanenko[a], T.A. Kharlamova[a], V.A. Kiselev[a], V.V. Kolmogorov[a], S.A. Kononov[a,b], K.Yu. Kotov[a], E.A. Kravchenko[a,b], V.N. Kudryavtsev[a,b], V.F. Kulikov[a,b], G.Ya. Kurkin[a,c], I.A. Kuyanov[a], E.A. Kuper[a,b], E.B. Levichev[a,c], D.A. Maksimov[a,b], V.M. Malyshev[a], A.L. Maslennikov[a,b], O.I. Meshkov[a,b], S.I. Mishnev[a], I.I. Morozov[a,b], N.Yu. Muchnoi[a,b], V.V. Neufeld[a], S.A. Nikitin[a], I.B. Nikolaev[a,b], I.N. Okunev[a], A.P. Onuchin[a,b,c], S.B. Oreshkin[a], A.A. Osipov[a,b], I.V. Ovtin[a,c], S.V. Peleganchuk[a,b], S.G. Pivovarov[a,c], P.A. Piminov[a], V.V. Petrov[a], V.G. Prisekin[a,b], O.L. Rezanova[a,b], A.A. Ruban[a,b], V.K. Sandyrev[a], G.A. Savinov[a], A.G. Shamov[a,b], D.N. Shatilov[a], B.A. Shwartz[a,b], E.A. Simonov[a], S.V. Sinyatkin[a], A.N. Skrinsky[a], A.V. Sokolov[a,b], A.M. Sukharev[a,b], E.V. Starostina[a,b], A.A. Talyshev[a,b], V.A. Tayursky[a,b], V.I. Telnov[a,b], Yu.A. Tikhonov[a,b], K.Yu. Todyshev[a,b,*], G.M. Tumaikin[a], Yu.V. Usov[a], A.I. Vorobiov[a], V.N. Zhilich[a,b], V.V. Zhulanov[a,b], A.N. Zhuravlev[a,b]

[a] *Budker Institute of Nuclear Physics, 11, akademika Lavrentieva prospect, Novosibirsk, 630090, Russia*
[b] *Novosibirsk State University, 2, Pirogova street, Novosibirsk, 630090, Russia*
[c] *Novosibirsk State Technical University, 20, Karl Marx prospect, Novosibirsk, 630092, Russia*

Abstract

Using the KEDR detector at the VEPP-4M e^+e^- collider, we have measured the values of $R_{\rm uds}$ and R at seven points of the center-of-mass energy between 3.12 and 3.72 GeV. The total achieved accuracy is about or better than 3.3% at most of energy points with a systematic uncertainty of about 2.1%. At the moment it is the most accurate measurement of $R(s)$ in this energy range.

1. Introduction

The quantity R is defined as the ratio of the radiatively corrected total hadronic cross section in electron-positron annihilation to the lowest-order QED cross section of the muon pair production. The precise $R(s)$ measurements are critical for determination of the value of the strong coupling constant $\alpha_s(s)$ and heavy quark masses [1], the anomalous magnetic moment of the muon $(g-2)_\mu$ and the value of the electromagnetic fine structure constant at the Z^0 peak $\alpha(M_Z^2)$ [2, 3].

Several experiments contributed to the $R(s)$ measurement in the energy range between 3.12 and 3.72 GeV [4, 5, 6, 7, 8, 9, 10, 11, 12]. The precision of these measurements does not exceed 5% for all experiments except BES-II [12], in which the accuracy of about 3.3% was reached at 3.07 and 3.65 GeV, but that is not enough for reliable calculation of the dispersion integrals in the whole energy range. It should be noted that systematic uncertainties dominate in all $R(s)$ measurements, thus there is good motivation for new experiments on the precise determination of $R(s)$ in this energy range, particularly important for $\alpha(M_Z^2)$.

In 2011 the region of the J/ψ and $\psi(2S)$ resonances was scanned in the KEDR [13] experiment with an integrated luminosity of about 1.4 pb^{-1}. In the data analysis presented below we tried to minimize correlations of systematic uncertainties with those in similar experiments by BES.

2. VEPP-4M collider and KEDR detector

The e^+e^- collider VEPP-4M [14] was designed to operate in the wide range of the beam energy 1÷5.5 GeV in the 2×2 bunches mode. The peak luminosity of VEPP-4M is about 2×10^{30} cm^{-2}s^{-1} in the vicinity of $\psi(2S)$.

The collider is well equipped for a precise beam energy determination. The beam energy in dedicated calibration runs is measured using the resonant depolarization method (RDM) [15, 16] with the relative accuracy of about 10^{-6}. The results of RDM calibrations can be interpolated to determine the energy during data taking with the accuracy of about 10 keV [17, 18]. Continuous energy monitoring is performed using the infrared light Compton backscattering [19] with the accuracy ~ 60 keV. The Compton backscattering also allows for the beam energy spread determination with the accuracy about 5%.

The KEDR detector is described in Ref. [13]. The detector consists of the vertex detector (VD), drift chamber (DC), time-of-flight (TOF) system of scintillation counters, particle identification system based on the aerogel Cherenkov counters, electromagnetic calorimeter (liquid krypton in the barrel part and CsI crystals in the endcaps), superconducting solenoid and muon system inside the magnet yoke. The superconducting solenoid provides a longitudinal magnetic field of 0.6 T. The detector is equipped with a tagging system of scattered electrons for two-photon studies. The on-line luminosity measurement is provided by two independent single bremsstrahlung monitors.

The trigger has two hardware levels: the primary (PT) and

*Corresponding author, e-mail: todyshev@inp.nsk.su

the secondary one (ST) [20]. The PT operates using signals from the TOF counters and fast signals from the CsI and LKr calorimeters, whereas the ST uses optimally shaped calorimeter signals and the information from VD, DC and the TOF system.

3. Experiment

The goal of the experiment was a measurement of the total hadronic cross section at seven equidistant points between 3.12 and 3.72 GeV. Two scans of the region were performed. The actual energies determined using the Compton backscattering method and the integrated luminosity at the points are presented in Table 1. The table also presents the relative contributions of the J/ψ and $\psi(2S)$ in the observed cross section dominated by their radiative tails. To determine them without external data, the additional data samples of about 0.4 pb^{-1} were collected at ten points in the peak regions. The data points and the resonance fits are shown in Fig. 1.

Table 1: Center-of-mass energy $\sqrt{s}$, integrated luminosity $\int\mathcal{L}dt$ and relative contribution of the J/ψ and $\psi(2S)$ resonances to the observed multihadronic cross section.

Point	$\sqrt{s}$, MeV	$\int\mathcal{L}dt$, nb^{-1}	$\frac{\sigma_{J/\psi}}{\sigma_{\rm obs}}$,%	$\frac{\sigma_{\psi(2S)}}{\sigma_{\rm obs}}$,%
		Scan 1		
1	3119.8 ± 0.2	64.31 ± 0.72	59.6	
2	3222.4 ± 0.2	74.79 ± 0.80	22.9	
3	3315.2 ± 0.2	83.25 ± 0.87	14.8	
4	3418.1 ± 0.2	95.68 ± 0.97	10.9	
5	3521.0 ± 0.2	112.36 ± 1.08	8.3	
6	3619.7 ± 0.2	34.72 ± 0.61	5.6	
7	3720.4 ± 0.2	55.57 ± 0.80	3.6	29.7
		Scan 2		
1	3120.1 ± 0.2	54.46 ± 0.63	58.3	
2	3223.6 ± 0.2	65.77 ± 0.88	23.0	
3	3313.9 ± 0.2	50.93 ± 0.61	14.9	
4	3418.4 ± 0.2	66.88 ± 0.88	10.4	
5	3520.3 ± 0.2	59.33 ± 0.67	7.9	
6	3617.6 ± 0.2	83.35 ± 0.95	5.6	
7	3718.9 ± 0.2	103.66 ± 1.05	3.5	30.5

The energies of the points in two scans are not the same because of the inaccuracy of the collider energy setting, but they are close enough to allow for summation of data samples.

4. Data analysis

4.1. Analysis procedure

The observed hadronic annihilation cross section was determined from

$$\sigma_{\rm obs}(s) = \frac{N_{\rm mh} - N_{\rm res.bg.}}{\int\mathcal{L}dt}, \qquad (1)$$

where $N_{\rm mh}$ is the number of events that pass hadronic selection criteria, $N_{\rm res.bg.}$ is the residual machine background evaluated as discussed in Sec. 4.6, and $\int\mathcal{L}dt$ is the integrated luminosity.

For the given observed cross section the R value was calculated as follows:

$$R = \frac{\sigma_{\rm obs}(s) - \sum\varepsilon_{\rm bg}(s)\,\sigma_{\rm bg}(s) - \sum\varepsilon_{\psi}(s)\,\sigma_{\psi}(s)}{\varepsilon(s)\,(1+\delta(s))\,\sigma^0_{\mu\mu}(s)}, \qquad (2)$$

where $\sigma^0_{\mu\mu}(s)$ is the Born cross section for $e^+e^-\to\mu^+\mu^-$ and $\varepsilon(s)$ is the detection efficiency for the single photon annihilation to hadrons. The second term in the numerator corresponds to the physical background from e^+e^-, $\mu^+\mu^-$ production, $\tau^+\tau^-$ production above threshold and two-photon processes. The third term represents a contribution of the J/ψ and $\psi(2S)$. Unlike Refs. [9, 10, 11, 12], we considered them explicitly instead of including in the radiation correction $\delta(s)$.

The detection efficiencies ε and $\varepsilon_{\rm bg}$ were determined from simulation. The efficiencies ε_{ψ} were found by fitting the resonance regions. The resonances were fitted separately in each scan, the free parameters were the detection efficiency at the world average values of the leptonic width Γ_{ee} and its product by the hadronic branching fraction $\mathcal{B}_h$, the machine energy spread and the magnitude of the continuum cross section observed at the reference point below the resonance. Calculations of a narrow resonance cross section and fits are described in more detail in Refs. [18, 21]. The J/ψ and $\psi(2S)$ detection efficiencies obtained and the χ^2 probabilities of the fits are presented in Table 2. The fitted values of the collision energy spread are also presented. They are not the same for the two scans because of variation of the accelerator regime, however, the energy spread is stable during a few days of operation in the resonant regions. The quoted values agree with the results of the energy spread determination using Compton backscattering within the accuracy provided by this method.

It should be noted that the tail cross section $\varepsilon_{\psi}(s)\,\sigma_{\psi}(s)$ depends on the $\varepsilon_{\psi}\Gamma_{ee}\mathcal{B}_h$ product and thus is not sensitive to the world average values of the leptonic width Γ_{ee} and the hadronic branching fraction $\mathcal{B}_h$ employed.

In our approach the radiative correction factor can be written as

$$1+\delta(s) = \int\frac{dx}{1-x}\,\frac{\mathcal{F}(s,x)}{\left|1-\tilde{\Pi}((1-x)s)\right|^2}\,\frac{\tilde{R}((1-x)s)\,\varepsilon((1-x)s)}{R(s)\,\varepsilon(s)}, \qquad (3)$$

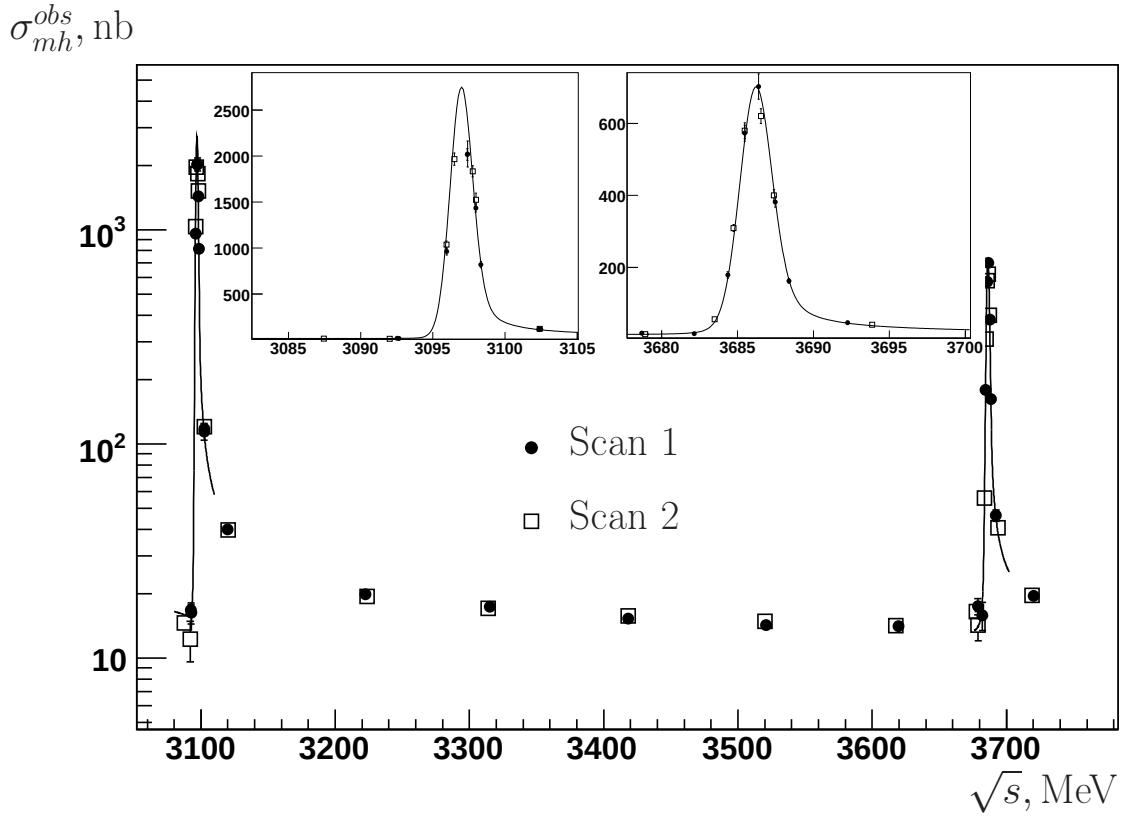

Figure 1: The observed multihadronic cross section as a function of the c.m. energy for the two scans. The curves are the result of the fits of the narrow resonances. The inserts show closeup of the J/ψ and $\psi(2S)$ regions.

Table 2: Efficiency, energy spread and χ^2 probability of the fits of the J/ψ and $\psi(2S)$ resonances (statistical errors only are presented).

	$\varepsilon_{J/\psi}$	$\sigma_W(J/\psi)$, MeV	$P(\chi^2)$, %	$\varepsilon_{\psi(2S)}$	$\sigma_W(\psi(2S))$, MeV	$P(\chi^2)$, %
Scan 1	0.760 ± 0.013	0.741 ± 0.005	77.6	0.838 ± 0.023	0.961 ± 0.033	44.9
Scan 2	0.751 ± 0.014	0.761 ± 0.007	18.5	0.830 ± 0.020	1.049 ± 0.054	73.3

where $\mathcal{F}(s,x)$ – the radiative correction kernel [22]. The variable x is a fraction of s lost due to initial state radiation. The vacuum polarization operator $\tilde{\Pi}$ and the quantity $\tilde{R}$ do not include a contribution of the J/ψ and $\psi(2S)$ resonances, details of the calculation are presented in Section 4.7.

It should be noted that in the approach described above we obtain the $R_{\rm uds}$ value. To get the quantity R, it is necessary to add the contribution of narrow resonances. In the following we shall use R instead of $R_{\rm uds}$ until Section 5.5.

4.2. Monte Carlo simulation

Simulation of the experiment was performed in the frame of the GEANT package, version 3.21 [23].

Single-photon annihilation to hadrons below $D\overline{D}$ threshold (uds continuum) was simulated using the JETSET 7.4 code [24, 25] with the parameters tuned at each energy point. As an alternative, we employed the LUARLW [26] generator which was kindly provided by the BES collaboration.

The results are presented in Fig. 2, where the most important event characteristics obtained in the experiment are compared with those in simulation. Good agreement is observed.

Bhabha events required for the precise luminosity determination were simulated using the BHWIDE generator [27]. The detection efficiencies for $\mu^+\mu^-$ and $\tau^+\tau^-$ events were obtained using the MC generator described in [28] and the KORALB event generator [29], respectively.

The $\psi(2S)$ and J/ψ decays were generated with the tuned version of the BES generator [30] based on the JETSET 7.4 code. The decay tables were updated according to the PDG edition 2010 [31]. Details of simulation of $\psi(2S)$ hadronic decays are discussed in Ref. [21].

Simulation reproduces most important event characteristics of the J/ψ hadronic decays. That allows us to introduce minor corrections to the detection efficiency of J/ψ hadronic decays presented in Table 2 required in the upper edge of the experiment energy range.

The two-photon processes $e^+e^- \to e^+e^-X$ are simulated with the generators described in Refs. [32, 33, 34].

4.3. Event selection and detection efficiencies

Both experimental and simulated events pass the software event filter during the offline analysis. That allows us to reduce systematic inaccuracy due to trigger instabilities and uncertainties in the hardware thresholds. The software filter recalculates the PT and ST decisions with stringent conditions using a digitized response of the detector subsystems.

To suppress the machine background to an acceptable level, the following PT conditions were used by OR:

- signals from ≥ two non-adjacent scintillation counters,
- signal from the LKr calorimeter,
- coincidence of the signals from two CsI endcaps.

Signals from two particles with the angular separation $\gtrsim 20^0$ should satisfy numerous ST conditions.

The MC simulation yields the trigger efficiency of about 0.95 for continuum uds production. Selection criteria

Table 3: Selection criteria for hadronic events which were used by AND.

Variable	Allowed range
$N^{\rm IP}_{\rm track}$	≥ 1
$E_{\rm obs}$	> 1.6 GeV
$E^{\rm max}_{\gamma}/E_{\rm beam}$	< 0.8
$E^{\rm tot}_{\rm cal}$	> 0.75 GeV
H_2/H_0	< 0.85
$\lvert P^{\rm miss}_{\rm z}/E_{\rm obs}\rvert$	< 0.6
$E_{\rm LKr}/E^{\rm tot}_{\rm cal}$	> 0.15
$\lvert Z_{\rm vertex}\rvert$	< 20.0 cm
$N_{\rm particles} \geq 4$ or $\tilde{N}^{\rm IP}_{\rm track} \geq 2$	

for multihadron events are listed in Table 3, and their description is provided below. Here N^{IP}_{track} is the number of tracks from a common vertex in the interaction region defined by: $\rho < 5$ mm, $|z_0| < 130$ mm, where ρ is the track impact parameter relative to the beam axis and z_0–coordinate of the closest approach point. The $\tilde{N}^{IP}_{track}$ is the number of tracks satisfying the conditions above with E/p less than 0.6, where E/p means the ratio of the energy deposited in the calorimeter to the measured momentum of the charged particle. The multiplicity $N_{\rm particles}$ is a sum of the number of charged tracks and the number of neutral particles detected in the calorimeters.

The observable energy $E_{\rm obs}$ is defined as a sum of the photon energies measured in the electromagnetic calorimeter and charged particle energies computed from the track momenta assuming pion masses. The observable energy cut and limitation on the ratio of the energy of the most energetic photon to the beam energy $E^{\rm max}_{\gamma}/E_{\rm beam}$ suppress production of hadronic events at low center-of-mass energies through initial state radiation and thus reduce the uncertainty of radiative corrections. The total calorimeter energy $E^{\rm tot}_{\rm cal}$ is defined as a sum of the energies of all clusters in the electromagnetic calorimeter. The cut on it suppresses background from cosmic rays. The cut on the ratio of Fox-Wolfram moments H_2/H_0 is efficient for suppression of the $e^+e^- \to e^+e^-\gamma$ background, that of cosmic rays and some kinds of the machine background. The background from two-photon and beam-gas events is suppressed by the cut on the ratio $|P^{\rm miss}_{\rm z}/E_{\rm obs}|$, where $P^{\rm miss}_{\rm z}$ is the z component of missing momentum . The background from beam-gas events was also suppressed by the cut on the ratio $E_{\rm LKr}/E_{\rm cal}$ of the energy deposited in the LKr calorimeter and total calorimeter energy. The event vertex position $Z_{\rm vertex}$ is the weighted average of the z_0's of the charged tracks. The cut on the $|Z_{\rm vertex}|$ suppresses background due to beam-gas, beam-wall and cosmic rays.

Table 4: Detection efficiency for the uds continuum in % (statistical errors only).

Point	ε_{JETSET}	ε_{LUARLW}	$\delta\varepsilon/\varepsilon$
Scan 1			
1	75.5 ± 0.1	75.0 ± 0.1	-0.7 ± 0.2
2	76.9 ± 0.1	76.2 ± 0.1	-0.9 ± 0.2
3	77.0 ± 0.1	77.0 ± 0.1	0.0 ± 0.2
4	78.1 ± 0.1	77.4 ± 0.1	-0.9 ± 0.2
5	78.3 ± 0.1	78.2 ± 0.1	-0.1 ± 0.2
6	79.6 ± 0.1	78.6 ± 0.1	-1.3 ± 0.2
7	80.8 ± 0.1	79.2 ± 0.1	-2.0 ± 0.2
Scan 2			
1	75.3 ± 0.1	74.9 ± 0.1	-0.5 ± 0.2
2	75.9 ± 0.1	75.1 ± 0.1	-1.1 ± 0.2
3	77.5 ± 0.1	77.3 ± 0.1	-0.3 ± 0.2
4	78.7 ± 0.1	78.0 ± 0.1	-0.9 ± 0.2
5	78.8 ± 0.1	78.7 ± 0.1	-0.1 ± 0.2
6	80.0 ± 0.1	79.0 ± 0.1	-1.3 ± 0.2
7	80.9 ± 0.1	79.4 ± 0.1	-1.9 ± 0.2

For additional suppression of the background induced by cosmic rays a veto from the muon system was required in the cases when more than two tracks did not cross the interaction region or the event arrival time determined by TOF relative to the bunch crossing was less than -7 ns or larger than 12 ns.

The detection efficiency for hadronic events corresponding to the selection criteria described above is presented in Table 4 for seven data points in which the *R* ratio was measured. It was determined using two versions of the event simulation.

4.4. Luminosity determination

The integrated luminosity at each point was determined using Bhabha events detected in the LKr calorimeter in the polar angle range $41^\circ < \theta < 159^\circ$. For the cross check we used Bhabha

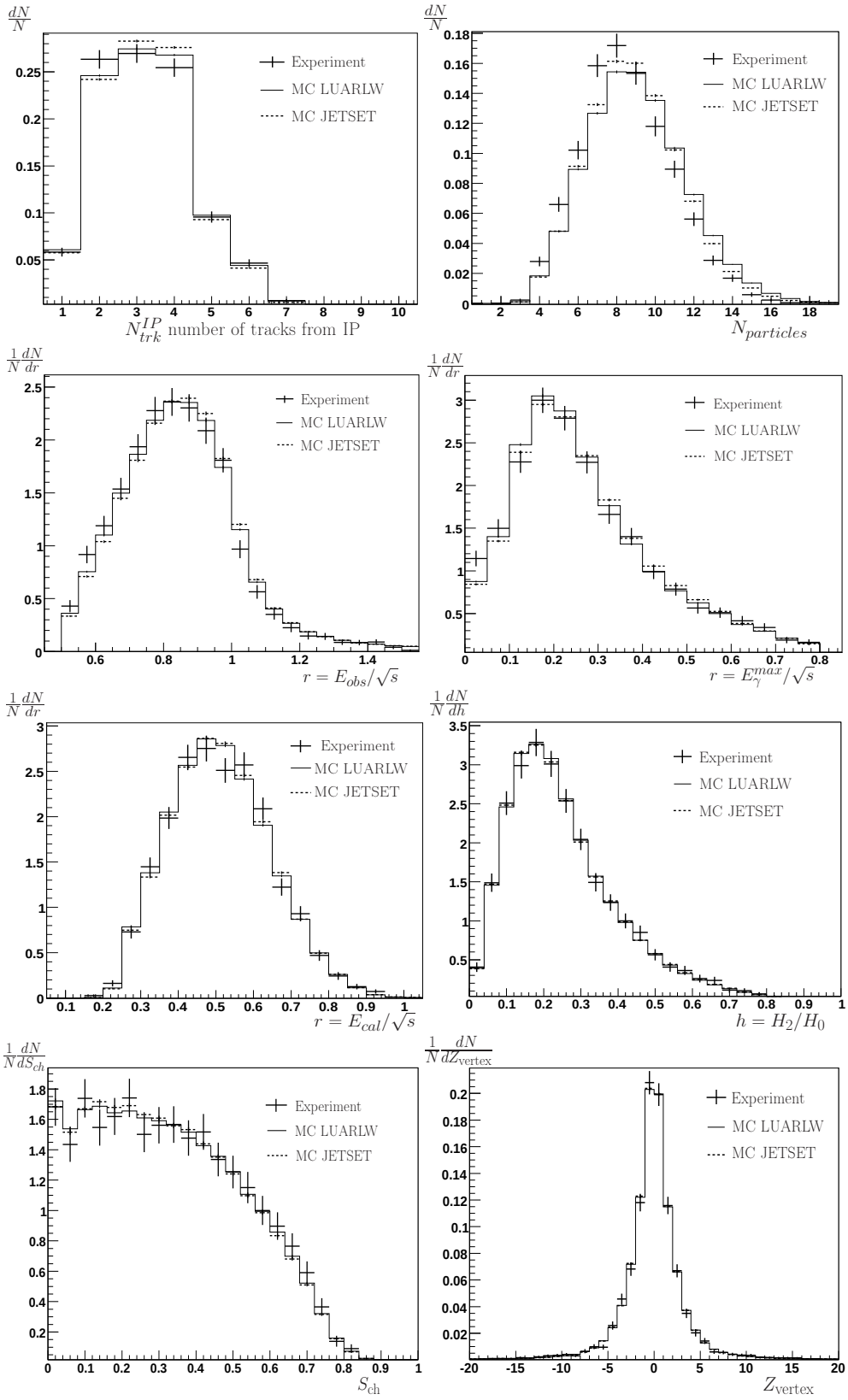

Figure 2: Properties of hadronic events produced in uds continuum at 3.12 GeV. Here N is the number of events, $S_{\rm ch}$ is sphericity, H_2 and H_0 are Fox-Wolfram moments. Integrals of all distributions are normalized to unity.

events in the endcap CsI calorimeter with $20^\circ < \theta < 32^\circ$ and $148^\circ < \theta < 160^\circ$.

The criteria for e^+e^- event selection are listed below:

- two clusters, each with the energy above 20% of the beam energy and the angle between them exceeding 162°,
- the total energy of these two clusters exceeds the beam energy,
- the calorimeter energy not associated with these two clusters does not exceed 20% of the total.

The tracking system was used only to reject the background from $e^+e^- \to \gamma\gamma$ and $e^+e^- \to hadrons$.

4.5. Physical background

To measure R values, we took into account the physical background contributions from the QED processes $e^+e^- \to e^+e^-$, $e^+e^- \to \mu^+\mu^-$ and $e^+e^- \to \tau^+\tau^-$. The sum of contributions from $e^+e^- \to e^+e^-$ and $e^+e^- \to \mu^+\mu^-$ production to the observed cross section is less than 0.1 nb. The uncertainties in the detection efficiency of $e^+e^- \to e^+e^-$ and $e^+e^- \to \mu^+\mu^-$ processes introduce about 0.1% uncertainty in the R value.

The contributions of $\tau^+\tau^-$ production are about 0.2 nb and 0.3 nb at two highest energy points, respectively, which induce a systematic uncertainty of less than 0.1% in the R ratio.

The two-photon interactions, which are the main source of background after $\tau^+\tau^-$ production, were studied with a simulation of $e^+e^- \to e^+e^-X$ events. We found that the contribution of two-photon events to the continuum cross section grows from 0.2% at 3.12 GeV to 0.5% at 3.72 GeV. The estimated uncertainty in the R value due to this contribution varies from 0.1% to 0.2%.

4.6. Correction for residual background

The contribution of residual machine background to the observed cross section was estimated using runs with separated e^+ and e^- bunches.

The residual background was evaluated and subtracted using the number of events which passed selection criteria in the background runs under the assumption that the background rate is proportional to the beam current and the measured vacuum pressure. As an alternative, we assumed that the background rate is proportional to the current only. The difference between the numbers of background events obtained with the two assumptions was considered as an uncertainty estimate at given energy point. The background values and their uncertainties at each energy point are presented in Table 5.

4.7. Radiative correction

The radiative correction factor was calculated according to Eq. (3) using the compilation of the vacuum polarization data by the CMD-2 group [36] and the relation between $R(s)$ and the hadronic part of the vacuum polarization $\Pi_{\rm hadr}(s)$:

$$R(s) = -\frac{3}{\alpha}\,\mathrm{Im}\,\Pi_{\rm hadr}(s). \qquad (4)$$

Table 5: The residual machine background in % of the observed cross section

Point	Scan 1	Scan 2
1	$1.3 \pm 0.2 \pm 0.4$	$1.3 \pm 0.2 \pm 0.4$
2	$2.4 \pm 0.4 \pm 0.5$	$2.7 \pm 0.4 \pm 0.5$
3	$2.7 \pm 0.5 \pm 0.4$	$3.0 \pm 0.5 \pm 0.4$
4	$2.9 \pm 0.5 \pm 0.4$	$3.6 \pm 0.6 \pm 0.4$
5	$3.1 \pm 0.6 \pm 0.5$	$3.3 \pm 0.5 \pm 0.5$
6	$2.7 \pm 0.5 \pm 0.4$	$3.7 \pm 0.6 \pm 0.4$
7	$2.1 \pm 0.4 \pm 0.2$	$2.2 \pm 0.3 \pm 0.2$

To calculate the operator $\tilde{\Pi}$ and the quantity $\tilde{R}$ for Eq. (3) we have subtracted analytically the contribution of the J/ψ and $\psi(2S)$ from data obtained by the CMD-2 group.

The dependence of the detection efficiency on the energy radiated in the initial state was simulated with the LUARLW generator which allowed us to simulate uds continuum below 3.12 GeV. The x dependence of the detection efficiency is shown in Fig. 3.

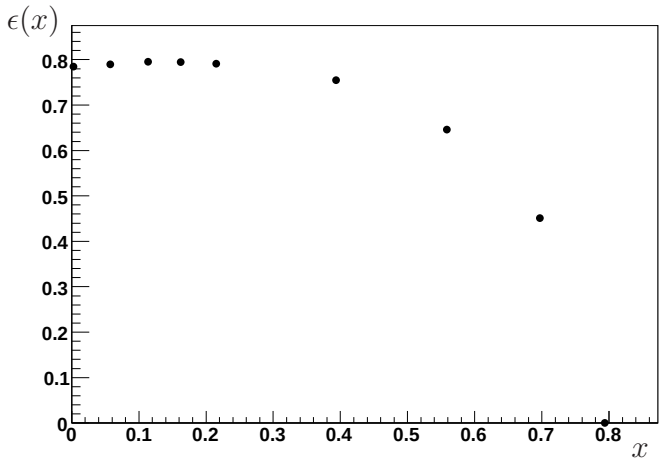

Figure 3: Hadronic detection efficiency versus variable x of Eq. (3) at 3.52 GeV in the first scan.

Table 6 contains values of the radiative correction and their systematic uncertainties which are discussed in Sec. 5.3.

4.8. J/ψ and $\psi(2S)$ contributions

To calculate contributions of narrow resonances to the observed cross section we used the detection efficiencies obtained from the fits. The values presented in Table 2 were corrected for the presence of ISR photons. The corrections were obtained via simulation of J/ψ and $\psi(2S)$ hadron decays at each energy point. These results are presented in Table 7. The systematic uncertainties of the J/ψ and $\psi(2S)$ detection efficiencies are due to the uncertainty in the beam energy determination and the detector instability.

Simulation of J/ψ hadron decays yields the detection efficiencies of 0.771 ± 0.001 and 0.767 ± 0.001 for two scans, respectively. The detection efficiencies obtained from simulation

Table 6: Radiative correction factor $1+\delta$

Point	Scan 1	Scan 2
1	1.0941 ± 0.0066	1.1074 ± 0.0066
2	1.0949 ± 0.0055	1.1049 ± 0.0055
3	1.0959 ± 0.0055	1.1100 ± 0.0056
4	1.0982 ± 0.0044	1.1094 ± 0.0044
5	1.1032 ± 0.0044	1.1102 ± 0.0044
6	1.1021 ± 0.0044	1.1098 ± 0.0044
7	1.1049 ± 0.0055	1.1067 ± 0.0055

Table 7: Detection efficiency for the J/ψ and $\psi(2S)$ hadronic decays of interest and its variation in the experiment energy range.

Resonance	Detection efficiency, %	$\Delta\varepsilon/\varepsilon$, %
	Scan 1	
J/ψ	$76.1 \pm 1.3 \pm 0.5$	$+1.2 \pm 0.1$
$\psi(2S)$	$83.8 \pm 2.3 \pm 0.9$	$+0.1 \pm 0.1$
	Scan 2	
J/ψ	$75.1 \pm 1.4 \pm 0.5$	$+1.3 \pm 0.1$
$\psi(2S)$	$83.0 \pm 2.0 \pm 0.9$	$+0.1 \pm 0.1$

of $\psi(2S)$ hadronic decays are 0.816 ± 0.001 and 0.817 ± 0.001 for two scans, respectively. For both resonances the detection efficiencies obtained by simulation agree with the fit results within the estimated errors.

4.9. Results of energy scans

The results of R measurement obtained in energy scans are presented in Table 8.

Table 8: Resulting R values with their statistical errors for two scans.

Point	Scan 1	Scan 2
1	2.194 ± 0.122	2.239 ± 0.131
2	2.195 ± 0.078	2.148 ± 0.082
3	2.233 ± 0.072	2.152 ± 0.089
4	2.152 ± 0.066	2.190 ± 0.078
5	2.173 ± 0.062	2.247 ± 0.086
6	2.209 ± 0.110	2.198 ± 0.070
7	2.195 ± 0.116	2.183 ± 0.084

5. Systematic uncertainties and results

5.1. Systematic uncertainty of absolute luminosity determination

The major contributions to the uncertainty of the absolute luminosity determination with the LKr calorimeter are presented in Table 9.

Table 9: Systematic uncertainties of the luminosity determination.

Source	Uncertainty, %
Calorimeter response	0.7
Calorimeter alignment	0.2
Polar angle resolution	0.2
Cross section calculation	0.5
Background	0.1
MC statistics	0.1
Variation of cuts	0.6
Sum in quadrature	1.1

The uncertainty due to the imperfect simulation of the calorimeter response was estimated by variation of relevant simulation parameters such as the accuracy of the electronic channel calibration, the geometrical factor controlling sensitivity to the energy loss fluctuations between calorimeter electrodes etc.

The LKr calorimeter was aligned with respect to the drift chamber using cosmic tracks reconstructed in the DC. The interaction point position and direction of the beam line were determined using the primary vertex distribution of multihadron events. The luminosity uncertainty due to inaccuracy of the alignment is less than 0.2%.

The difference in the polar angle resolutions observed in experiment and predicted by simulation causes an uncertainty in the luminosity measurement, because events migrate into or out of the fiducial volume.

The uncertainty of the theoretical Bhabha cross section was estimated comparing the results obtained with the BHWIDE [27] and MCGPJ [35] event generators. It agrees with the errors quoted by the authors.

The background to the Bhabha process from the J/ψ and $\psi(2S)$ decays and reactions $e^+e^- \to \mu\mu(\gamma)$ and $e^+e^- \to \gamma\gamma$ was estimated using MC simulation. It contributes less than 0.2% to the observed e^+e^- cross section at seven energy points presented in Table 1. At the auxiliary points of the scan serving for the determination of the J/ψ and $\psi(2S)$ signal magnitude the contributions of the resonance decays to e^+e^- were accounted for in the fits. We also considered a contribution of residual machine background to Bhabha events which is about 0.1%. The residual luminosity uncertainty due to background does not exceed 0.1%.

To evaluate the effect of other possible sources of systematic uncertainty, the variation of the cuts was performed within the fiducial region in which good agreement between the MC simulation and experiment is observed.

Differences of integrated luminosities obtained using the LKr and CsI calorimeters in two scans are $0.5 \pm 0.5\%$ and $0.0 \pm 0.5\%$, respectively. That is consistent with the estimates in Table 9.

5.2. Uncertainty due to imperfect simulation of continuum

The imperfect simulation of uds continuum contributes significantly to the systematic uncertainty in R. Considering the detection efficiencies reported in Table 4 obtained with the JETSET and LUARLW hadronic generators one can evaluate the systematic uncertainty related to the detection efficiency. The maximal deviation of 1.3% is taken as the systematic uncertainty for the energy range 3.12-3.62 GeV. Our estimate of the systematic uncertainty due to the uds continuum generator is more conservative than the value 0.5% used in Ref. [12] with the LUARLW generator in this energy range. At the energy of 3.72 GeV our estimation of this uncertainty is 2%.

There is a systematic uncertainty in the observed multiplicity related to the track reconstruction efficiency, which is not exactly the same for the experimental data and simulation. The multiplicity together with other event parameters was employed for the JETSET parameter tuning limiting the tuning accuracy. The reconstruction efficiency was studied using Bhabha events and low-momentum cosmic tracks and the appropriate correction was introduced in the MC simulation. The uncertainty of the correction introduces the additional systematic uncertainty of about 0.5%.

The contributions to the detection efficiency uncertainty due to imperfect simulation of uds continuum are summarized in Table 10.

Table 10: Systematic uncertainties of the detection efficiency due to uds continuum simulation.

Source	Uncertainty, %	
	Points 1-6	Point 7
uds simulation	1.3	2.0
Track reconstruction	0.5	0.5
MC statistics	0.2	0.2
Sum in quadrature	1.4	2.1

5.3. Systematic uncertainty of the radiative correction

The main sources of systematic uncertainty in the radiative correction factor at each energy point are listed in Table 11. The four contributions were evaluated and summed up in quadrature.

To estimate the uncertainty related to a choice of the vacuum polarization operator approximation, that from CMD-2 [36] was replaced with the approximation employed in the BES generator [30]. The variation reaches 0.4% at the points closest to J/ψ and $\psi(2S)$ and drops down to 0.1% at the other points. The contribution denoted as $\delta R(s)$ is related to the $R(s)$ uncertainty. It is less than 0.5% for the entire energy range. The contribution $\delta\varepsilon(s)$ of about 0.2% is related to the uncertainty in the $\varepsilon(s)$ dependence. A calculation of the radiative corrections according to Eq. (3) requires the interpolation of the detection efficiency presented in Fig. 3 as a function of x. The contribution $\delta_{\rm calc}$ is due to the relatively small number of points where the efficiency was calculated by Monte Carlo. It was estimated comparing the results obtained using the linear interpolation and the quadratic one.

Table 11: Systematic uncertainties of the radiative correction.

Point	Uncertainty, %				
	Contributions				Total
	Π approx.	$\delta R(s)$	$\delta\varepsilon(s)$	δ_{calc}	
1	0.3	0.5	0.2	0.2	0.6
2	0.1	0.4	0.2	0.2	0.5
3	0.1	0.4	0.2	0.2	0.5
4	0.1	0.3	0.2	0.2	0.4
5	0.1	0.3	0.2	0.2	0.4
6	0.1	0.3	0.2	0.2	0.4
7	0.4	0.3	0.2	0.2	0.5

5.4. Detector-related uncertainties in R

The systematic uncertainties related to the efficiency of the track reconstruction were considered in Sec. 5.2.

The main source of the trigger efficiency uncertainty is that of the calorimeter thresholds in the secondary trigger. The estimate of about 0.2% was obtained varying the threshold in the software event filter.

The trigger efficiency and the event selection efficiency depend on the calorimeter response to hadrons. The uncertainty related to the simulation of nuclear interaction was estimated by comparison of the efficiencies obtained with the packages GHEISHA [37] and FLUKA [38] which are implemented in GEANT 3.21 [23]. The relative difference was about 0.2%.

The effect of other possible sources of the detector-related uncertainty was evaluated by varying the event selection cuts that are presented in Table 12. All variations of R observed were smaller than their statistical errors and can originate from the already considered sources of uncertainties or the statistical fluctuations, nevertheless we included them in the total uncertainty to obtain conservative error estimates.

Table 12: R uncertainty due to variation of the selection criteria for hadronic events.

Variable	Range variation	R variation in %
$E_{\rm obs}$	$> 1.4 \div 1.8$ GeV	0.3
$E_\gamma^{\rm max}/E_{\rm beam}$	$< 0.6 \div 0.9$	0.3
$E_{\rm cal}^{\rm tot}$	$> 0.5 \div 0.75$ GeV	0.2
H_2/H_0	$< 0.75 \div 0.9$	0.3
$\lvert P_{\rm z}^{\rm miss}/E_{\rm obs}\rvert$	$< 0.6 \div 0.8$	0.2
$E_{\rm LKr}/E_{\rm cal}^{\rm tot}$	$> 0.15 \div 0.25$	0.1
$\lvert Z_{\rm vertex}\rvert$	$< 20.0 \div 15.0$ cm	0.2
Sum in quadrature		0.6

Table 13: $R_{\rm uds}$ systematic uncertainties (in %) assigned to each energy point.

	Point 1	Point 2	Point 3	Point 4	Point 5	Point 6	Point 7
Luminosity	1.1	1.1	1.1	1.1	1.1	1.1	1.1
Radiative correction	0.6	0.5	0.5	0.4	0.4	0.4	0.5
Continuum simulation	1.4	1.4	1.4	1.4	1.4	1.4	2.1
e^+e^-X contribution	0.1	0.1	0.1	0.2	0.2	0.2	0.2
l^+l^- contribution	0.1	0.1	0.1	0.1	0.1	0.2	0.2
Trigger efficiency	0.2	0.2	0.2	0.2	0.2	0.2	0.2
Nuclear interaction	0.2	0.2	0.2	0.2	0.2	0.2	0.2
Cuts variation	0.6	0.6	0.6	0.6	0.6	0.6	0.6
Scan 1							
J/ψ and $\psi(2S)$ contribution	2.7	0.5	0.3	0.2	0.2	0.1	1.4
Machine background	1.1	0.8	0.7	0.7	0.9	0.7	0.7
Sum in quadrature	3.5	2.2	2.1	2.1	2.2	2.1	3.0
Scan 2							
J/ψ and $\psi(2S)$ contribution	2.8	0.6	0.3	0.2	0.2	0.1	1.3
Machine background	1.1	0.8	0.7	0.8	0.8	0.7	0.5
Sum in quadrature	3.6	2.2	2.1	2.1	2.1	2.1	2.9
Correlated in two scans	2.3	1.9	1.8	1.8	1.8	1.8	2.5

5.5. Summary of systematic uncertainties and results

The major sources of the systematic uncertainty on the $R_{\rm uds}$ value are listed in Table 13.

At each energy point we divide the systematic uncertainty into a common uncertainty that is correlated in two scans for given energy and uncorrelated uncertainty that is independent for each scan. During data collection at given energy point the relative beam energy variation was less than 10^{-3} allowing us to neglect this source of uncertainty.

As mentioned above, the contribution of narrow resonances to $R(s)$ is not negligible in the resonance region. This contribution was found analytically using "bare" parameters of the resonances, which were calculated based on the PDG data [39].

The results of the two scans were weighted using their statistical uncertainties and the uncorrelated parts of the systematic ones. The formal description of the weighting procedure can be found in Ref. [21]. The obtained $R_{\rm uds}$ and R values as well as luminosity-weighted average center-of-mass energies are presented in Table 14.

The inaccuracy of R associated with the resonance parameters is negligible in comparison with the others uncertainties, so the errors for the values of R and $R_{\rm uds}$ are the same.

Table 14: Measured values of $R_{\rm uds}(s)$ and $R(s)$ with statistical and systematic uncertainties.

$\sqrt{s}$, MeV	$R_{\rm uds}(s)$ $\{R(s)\}$
3119.9 ± 0.2	$2.215\{2.237\} \pm 0.089 \pm 0.066$
3223.0 ± 0.6	$2.172\{2.173\} \pm 0.057 \pm 0.045$
3314.7 ± 0.7	$2.200\{2.200\} \pm 0.056 \pm 0.043$
3418.2 ± 0.2	$2.168\{2.168\} \pm 0.050 \pm 0.042$
3520.8 ± 0.4	$2.200\{2.201\} \pm 0.050 \pm 0.044$
3618.2 ± 1.0	$2.201\{2.207\} \pm 0.059 \pm 0.044$
3719.4 ± 0.7	$2.187\{2.211\} \pm 0.068 \pm 0.060$

6. Summary

We have measured the R and $R_{\rm uds}$ values at seven center-of-mass energies between 3.12 and 3.72 GeV. At most of the energy points the achieved accuracy is about or better than 3.3% at the systematic uncertainty 2.1%. The R values are consistent within errors with the BES results [12] and provide more detailed information on the $R(s)$ quantity in this energy range.

The weighted average $\overline{R}_{\rm uds} = 2.189 \pm 0.022 \pm 0.042$ agrees well with $R = 2.16 \pm 0.01$ calculated according to the pQCD expansion [40] for $\alpha_s(m_\tau) = 0.333 \pm 0.013$ obtained from hadronic τ decays [41]. The results are shown in Fig. 4.

It is worth noting that while calculating the dispersion integrals in this energy range it is preferable to use the measured $R_{\rm uds}(s)$ values adding the contribution of narrow resonances calculated analytically. Using the full R values in this case leads to some double counting.

Acknowledgments

We greatly appreciate the efforts of the staff of VEPP-4M to provide good operation of the complex during long term experiments. The authors are grateful to V. P. Druzhinin for useful discussions.

This work has been supported by Russian Science Foundation (project N 14-50-00080).

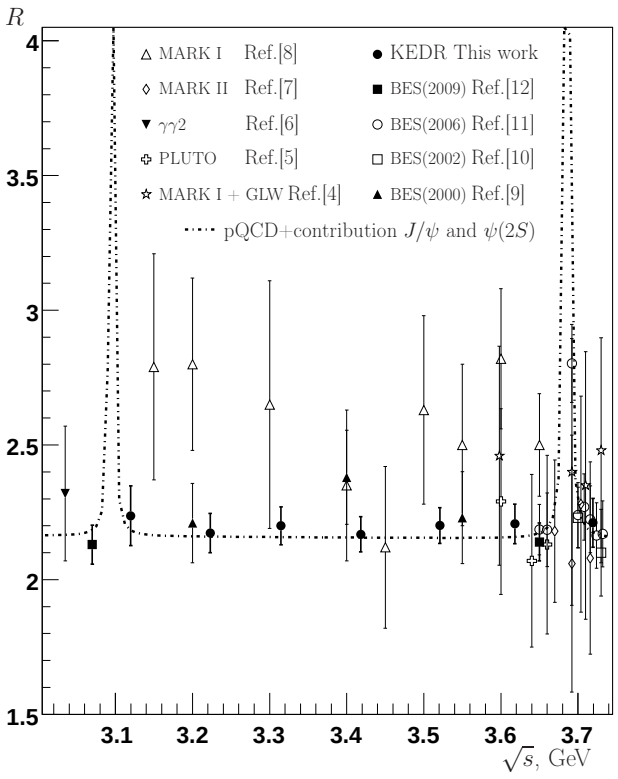

Figure 4: The quantity R versus the c.m. energy and the sum of the prediction of perturbative QCD and a contribution of narrow resonances.

References

[1] N. Brambilla *et al.,* Eur. Phys. J. C **71**, 1534 (2011).
[2] M. Davier *et al.,* Eur. Phys. J. C **71**, 1515 (2011).
[3] K. Hagiwara *et al.,* J. Phys. J. G **38**, 085003 (2011).
[4] P. A. Rapidis *et al.,* Phys. Rev. Lett. **39**, 526 (1977).
[5] J. Burmester *et al.,* Phys. Lett. B **66**, 395 (1977).
[6] C. Bacci *et al.,* Phys. Lett. B **86**, 234(1979).
[7] R. H. Schindler *et al.,* Phys. Rev. D **21**, 2716 (1980).
[8] J. L. Siegrist *et al.,* Phys. Lett. B **26**, 969 (1982).
[9] J. Z. Bai *et al.* (BES Collaboration), Phys. Rev. Lett. **84**, 594 (2000).
[10] J. Z. Bai *et al.* (BES Collaboration), Phys.Rev.Lett. **88**, 101802 (2002).
[11] M. Ablikim *et al.* (BES Collaboration), Phys. Rev. Lett. **97**, 262001 (2006).
[12] M. Ablikim *et al.* (BES Collaboration), Phys. Lett. B **677**, 239 (2009).
[13] V. V. Anashin *et.al.,* Phys. of Part. and Nucl. **44**, 657 (2013).
[14] V. V. Anashin *et al.,* Stockholm 1998, EPAC 98*, 400 (1998).
[15] A. D. Bukin *et al.,* Absolute Calibration of Beam Energy in the Storage Ring. Phi-Meson Mass Measurement, Preprint IYF-75-64, 1975.
[16] A. N. Skrinsky and Y. M. Shatunov, Sov. Phys. Usp. **32**, 548 (1989).
[17] V. M. Aulchenko *et al.* (KEDR Collaboration), Phys. Lett. B **573**, 63 (2003).
[18] V. V. Anashin *et al.* (KEDR Collaboration), Phys. Lett. B **749**, 50 (2015).
[19] V. E. Blinov *et al.,* ICFA Beam Dyn. Newslett. **48**, 195 (2009).
[20] S. E. Baru *et al.*, Instrum. Exp. Tech. **54**, 335 (2011).
[21] V. V. Anashin *et al.* (KEDR Collaboration), Phys. Lett. B **711**, 280 (2012).
[22] E. A. Kuraev and V. S. Fadin, Sov. J. Nucl. Phys. **41**, 466 (1985).
[23] GEANT – Detector Description and Simulation Tool CERN Program Library Long Writeup W5013.
[24] T. Sjostrand, M. Bengtsson, Comp. Phys. Comm. **43**, 367 (1987).
[25] T. Sjostrand, S. Mrenna, P. Skands, PYTHIA 6.4 Physics and Manual, arXiv:hep-ph/0603175.
[26] Haiming Hu and An Tai, arXiv:hep-ex/0106017.
[27] S. Jadach, W. Placzek, B. F. L. Ward, Phys. Lett. B **390**, 298 (1997).
[28] F. A. Berends *et al.,* Comp. Phys. Comm. **29**, 185 (1983).
[29] S. Jadach, Z. Was, Comp. Phys. Comm. **85**, 453 (1995).
[30] J. C. Chen *et al.,* Phys. Rev. D **62**, 034003 (2000).
[31] K. Nakamura *et al.* (PDG), J. Phys. G **37**, 075021 (2010).
[32] F. A. Berends *et al.,* Comp. Phys. Comm. **40**, 285 (1986).
[33] F. A. Berends *et al.,* Comp. Phys. Comm. **40**, 271 (1986).
[34] V.A.Tayursky, S.I.Eidelman, Preprint IYaF 2000-78, Novosibirsk 2000 (in Russian).
[35] A. B. Arbuzov *et al.,* Eur. Phys. J. C **46**, 689 (2006).
[36] S. Actis *et al.*, Eur. Phys. J. C **66**, 585 (2010).
[37] H.C. Fesefeldt, Technical Report PITHA-85-02, III Physilakisches Institut, RWTH Aachen Physikzentrum, 5100 Aachen, Germany, Sep. 1985.
[38] A. Fassò *et al.,* Talk at the Computing in High Energy and Nuclear Physics (CHEP03), arXiv:physics/0306162.
[39] K. A. Olive *et al.*(PDG), Chin. Phys. C **38**, 090001 (2014).
[40] P. A. Baikov *et al.,* Phys. Lett. **B 714**, 62 (2012).
[41] N. Brambilla *et al.,* Eur. Phys. J. C **74**, 2981 (2014).